Berg Huettenmaenn Monatsh (2023) Vol. 168 (5): 247–253
https://doi.org/10.1007/s00501-023-01346-3

BHM Berg- und Hüttenmännische Monatshefte

High Temperature Tensile Strength of TI6AL4V Processed by L-PBF—Influence of Microstructure and Heat Treatment

Benjamin Meier[1,2], Fernando Warchomicka[2], Jelena Petrusa[1], Reinhard Kaindl[1], Wolfgang Waldhauser[1], and Christof Sommitsch[2]

[1]Joanneum Research—Materials, Niklasdorf, Austria
[2]IMAT Institute of Material Science, Joining and Forming, University of Technology, Graz, Austria

Received March 9, 2023; accepted March 27, 2023; published online May 25, 2023

Abstract: Ti6Al4V is the most widely used α-β Titanium alloy for application in medicine, automotive, and aerospace, known for its high strength and corrosion resistance, but also its high maximal operating temperature of around 420 °C. Combined with its decent weldability under a shield atmosphere it has become a standard alloy for additive manufacturing processes, especially laser and electron beam powder bed fusion (L-PBF). Although this material is well studied, the influence of the L-PBF process on its tensile properties at elevated temperatures remains almost unexplored. For that reason, this contribution focuses on the analysis of the tensile properties of Ti6Al4V up to 500 °C for different heat treatments and compares it to aerospace standards.
Furnace annealed samples reach a tensile strength between 1022 to 660 MPa from room temperature to 500 °C respectively, while stress-relieved specimens reach 1205 to 756 MPa. Stress-relieved samples show a lower ductility at room temperature, but elongation at break increases at high temperature and outperforms furnace annealed samples at 500 °C.

Keywords: L-PBF, SLM, High temperature, Tensile strength, Heat treatment

Hochtemperatur-Zugfestigkeit von TI6AL4V, verarbeitet mit L-PBF – Einfluss von Mikrostruktur und Wärmebehandlung

Zusammenfassung: Ti6Al4V ist die am weitesten verbreitete α-β-Titanlegierung für Anwendungen in der Medizin, im Automobilbau und in der Luft- und Raumfahrt. Sie ist bekannt für ihre hohe Festigkeit und Korrosionsbeständigkeit, aber auch für ihre hohe maximale Betriebstemperatur von etwa 420 °C. In Verbindung mit ihrer guten Schweißbarkeit unter Schutzgasatmosphäre wurde sie zu einer Standardlegierung für additive Fertigungsverfahren, insbesondere für das Laser- und Elektronenstrahl-Pulverbettschweißen (L-PBF). Obwohl dieser Werkstoff gut erforscht ist, bleibt der Einfluss des L-PBF-Prozesses auf seine Zugeigenschaften bei erhöhten Temperaturen nahezu unerforscht. Aus diesem Grund konzentriert sich diese Arbeit auf die Analyse der Zugfestigkeit von Ti6Al4V bis 500 °C bei verschiedenen Wärmebehandlungen und vergleicht sie mit den Normen der Luft- und Raumfahrt.
Warmausgelagerte Proben erreichen eine Zugfestigkeit zwischen 1022 und 660 MPa von Raumtemperatur bis 500 °C, während spannungsarmgeglühte Proben 1205 bis 756 MPa erreichen. Spannungsarmgeglühte Proben weisen bei Raumtemperatur eine geringere Duktilität auf, aber die Bruchdehnung nimmt bei hohen Temperaturen zu und übertrifft bei 500 °C die der warmausgelagerten Proben.

Schlüsselwörter: L-PBF, SLM, Hochtemperatur, Zugfestigkeit, Wärmebehandlung

1. Introduction

Ti6Al4V Grade 5 (Ti64) is the most widely used titanium alloy and is well established in additive manufacturing, especially Laser Powder Bed Fusion (L-PBF). Due to the alloy's high strength-to-weight ratio and excellent corrosion resistance, it finds applications in medical implants and automotive, but most importantly in aerospace—wherever the properties of the material outplay the costs and processing.

Especially in aerospace applications, such as gas turbine engines and adjected components, the strength of Ti64 at elevated temperature is of high interest since its density is nearly half of the otherwise used high-temperature resistant Ni-Superalloys [1, 2]. For classically wrought, forged, and machined Ti64, the maximal service temperature is

B. Meier (✉)
Joanneum Research—Materials,
Leobnerstraße 94,
8712 Niklasdorf, Austria
benjamin.meier@joanneum.at; b.meier@student.tugraz.at

limited by the poor oxidation resistance at temperatures higher than 400 °C. An increased oxygen intake leads to the formation of α case, loss in ductility and fatigue strength [1, 2]. Therefore, the MMPDS standard suggests its use up to 400 °C [3], as do Lütjering and Williams [2].

However, metals processed by L-PBF show a different fine-grained, often anisotropic, and microstructure compared to their wrought, forged, and machined counterparts due to build-process direction and high cooling rates [4–8].

He et al. [9] show the influence of anisotropy on the creep behavior at 450 and 600 °C and tensile strength at room temperature after a thermal exposure of 200 h at 500 and 600 °C for furnace annealed α + β specimens and compare it to forged samples for the same thermal exposure. It shows a high anisotropic effect of temperature on ductility and creep, but with strength values higher than forged samples. Viespoli et al. [10] investigate creep [450, 500, and 600 °C] and fatigue behavior at 600 °C for as-build martensitic samples. It shows a high decrement in high cycle fatigue performance, however, creep strength(unclear) on the level of forged billets without any definition of their heat treatment and microstructure. The work of Muiruri et al. [11] investigates the impact toughness of Ti64 Grade 23 from –150 to 250 °C and shows a transition from brittle to ductile behavior, highly influenced by heat treatment applied. Zhao et al. [12] performed selected tensile tests for as-build not stress-relieved samples where the specimens were cut out of bulk material and no further information on the print direction of the specimens was tested. While very brittle, it shows an increase of ductility up to 350 °C and a decrease afterward, reaching the same elongation at break at RT and 400 °C.

Additional creep results for materials processed by L-PBF can be found for Ni-Superalloys [13, 14]. Due to their complex microstructure, cast materials are superior and the same anisotropy as with Ti-Alloys can be observed. Rao et al. [15] investigated the hot impression creep behavior of AlSi10Mg showing a three times increase in the indentation at 100 °C for solution heat treatment, but there is no comparison to classically produced alloy.

The scope of this contribution is to investigate the tensile strength of Ti64 within the range of allowed operating temperature from RT to 500 °C. This is done for two different heat treatments and microstructural conditions, martensitic α′ and α + β respectively, to investigate possible advantages of the higher strength of α′ at high temperatures, since near α alloys can be used up to 600 °C [1, 2].

2. Methodology

Specimens were built on an EOS Eosint M280 L-PBF machine equipped with a 400 W Ng:YAg Laser. Process parameters can be found in Table 1.

Only virgin powder from a single production batch was used, whose verified properties [16] are shown in Table 2, all within Grade 5 limits according to ASTM B265. This is done to ensure that changes in powder properties within the powder reuse do not affect the results [17, 18].

All specimens underwent post-process stress relief heat treatment (2 h at 650 °C) in an Argon-flooded Lynntherm furnace. Additional furnace annealing (2 h at 800 °C) was carried out in a vacuum furnace to compare properties with stress relief condition. Related microstructures are shown in Fig. 1 and can be found in the previous work of Meier et al. [16], where the same powder batch was investigated.

TABLE 1
L-PBF process parameters

Laser Power	Scan Speed	Hatching	Layer Thickness	Energy Input
[W]	[mm/s]	[µm]	[µm]	[J/mm^3]
280	1200	140	30	55.6

TABLE 2
Chemical composition, particle size distribution, and morphology of the powder used

Chemical Composition						Particle Size Distribution			Morphology		
Al	V	O	N	Ar	H	D10	D50	D90	Sphericity	Carney Flow	Bulk Density
[wt.%]	[wt.%]	[wt.%]	[wt.%]	[ppm]	[ppm]	[µm]	[µm]	[µm]	[W/H]	[s/50 g]	[g/cm^3]
6.13	3.9	0.16	0.03	1.1	21	18.8	33.6	48.7	0.89	8.4	2.34

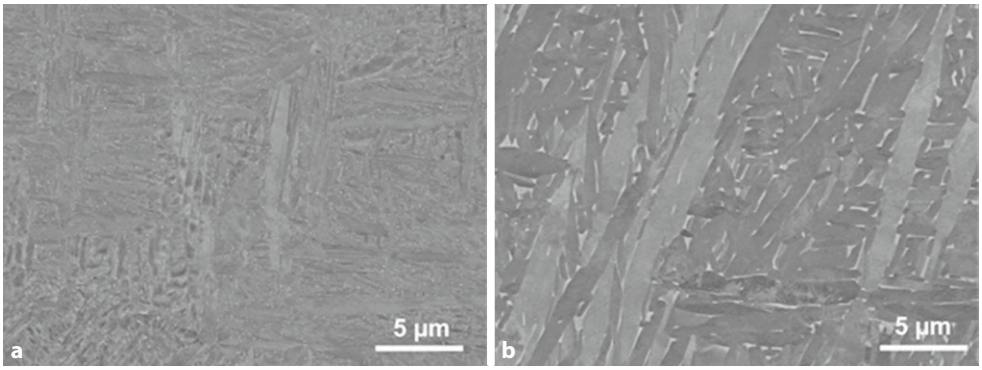

Fig. 1: Microstructure after **a** stress relief and **b** furnace annealing [18]

Stress relief led to partially decomposed martensitic microstructure with a small β phase (Fig. 1a), while furnace annealing achieved stabilized and coarser α laths within the β phase (Fig. 1b; [18]).

Tensile tests at elevated temperature were carried out on a Gleeble 3800 test machine with ohmic heating system. Samples were clamped using conical copper holders to provide high conductivity and temperature is controlled by at least two S-Type thermocouples welded to the middle (C1) and end (C2 and C3) of the gauge length (Fig. 2).

Table 3 shows the matrix of experiment used in this study. For the tensile tests, the samples were heated at 5 K/s and then hold for 1 min before the deformation. Tensile test were controlled by the stroke with a displacement rate of 1 mm/min.

The specimens' gauge length was designed according to ASTM 8 as depicted in Fig. 2a, while the clamping was adopted to the Gleeble machine. Due to comparability to ASTM E8, tests at RT, 90°, and 120 °C were performed according to the named standard, at RT on a Zwick Roell test rig (3b), and the others on an Instron 8802/8802K9832 test rig using an Instron CP107081 temperature chamber. Threaded specimens (Fig. 3c) were used. All samples are built in vertical orientation since anisotropy in tensile strength was negligible for the material and ductile anisotropy ought to be similar to the behavior found in [15] and [19].

TABLE 3
Test Matrix

Temperature [C°]	Specimen and Heat Treatment			
	Gleeble		ASTM E8	
	Stress Relief	Furnace Annealed	Stress Relief	Furnace Annealed
RT (25 °C)	2	3	5	5
90	2	5	–	5
120	–	5	–	5
200	2	3	–	–
300	2	2	–	–
400	2	2	–	–
500	3	3	–	–

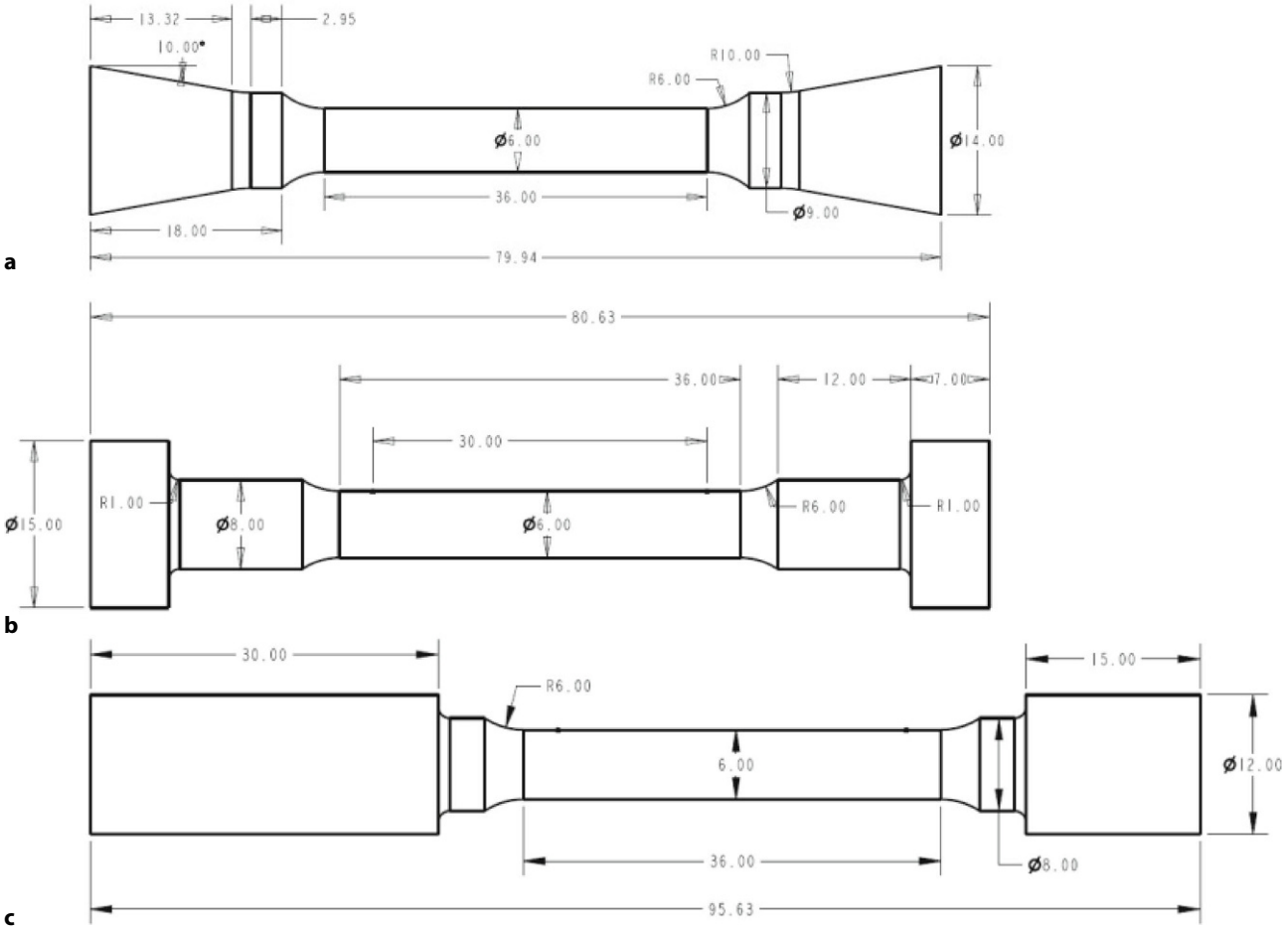

Fig. 2: Cylindrical specimen design for **a** Gleeble **b** Zwick Roell, and **c** Instron test rig with clamping mechanically turned to M10

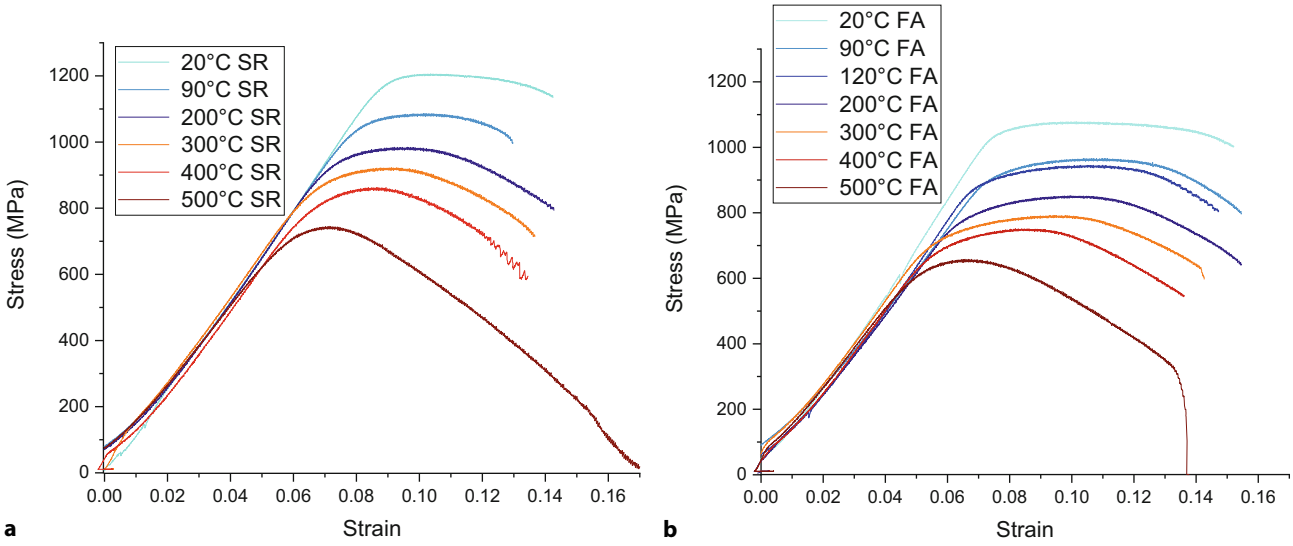

Fig. 3: Stress-strain diagrams for **a** stress relieved and **b** furnace annealed samples for all investigated temperatures

3. Results and Discussion

Figure 3a, b shows representative stress-strain curves for stress-relieved (3a) and furnace annealed (3b) samples performed on the Gleeble machine.

For both heat treatments, the strength decreases with increasing temperature. In Fig. 4, the ultimate tensile and yield strength of performed tests are compared to standard values found in MMPDS material data sheets as well as tests fully according to ASTM E8 performed with the same material. Both stress-relieved and furnace annealed samples exceed the values for standard material. Out of MMPDS standard, furnace annealed bar and sheet material < 1.72 mm (AMS4928) was selected as it was found to be closest to the tested specimen.

Stress-relieved samples reach a tensile strength of around 120 MPa more than furnace annealed ones and 260 MPa higher than the values found in MMPDS data sheets. Yield strength for both heat treatments is about 80 MPa below ultimate strength and decreases faster till 400 °C. From 400 °C to 500 °C, they seem to stabilize, while the ultimate tensile strength further decreases. A similar effect can be seen in the MMPDS. Measurements according to ASTM E8 are comparable to those of the Gleeble machine.

The maximal strain reached over raising temperature can be seen in Fig. 5. Both heat treatments show a decrease in ductility for 90 °C from where elongation at break increases up to 200 °C to decrease again with rising temperature. However, these changes are within the deviation, shown in Table 4. While more brittle than furnace annealed from room temperature to 400 °C the stress-relieved specimen show increased plastic break behavior at 500 °C reaching a maximum strain of 0.169, when furnace annealed samples drop further to a maximum strain of 0.128. The elongation reached is in between the expected values for furnace annealed bar (Fig. 5, yellow line) and sheet (Fig. 5, green line) material found in MMPDS data sheets. Both

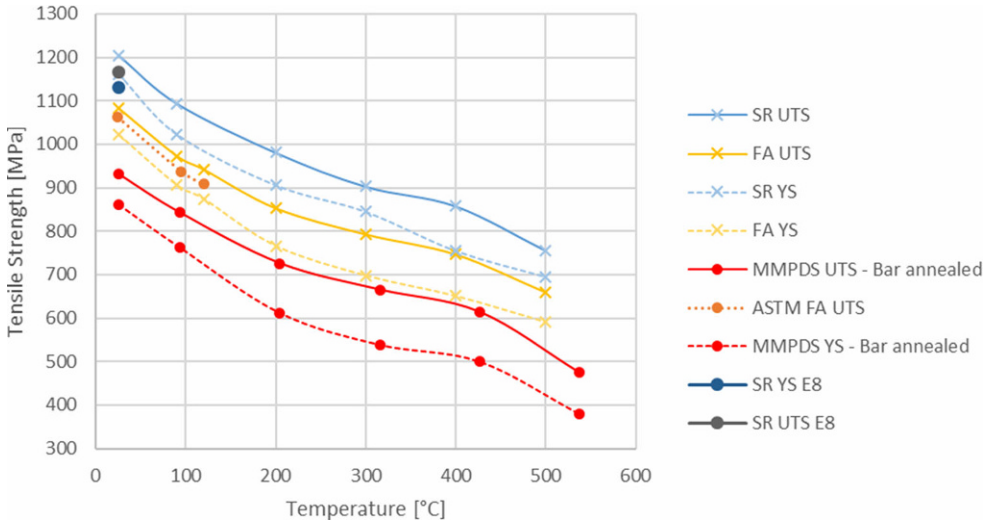

Fig. 4: Yield strength (*YS*) and ultimate tensile strength (*UTS*) for stress-relieved (*SR*) and furnace annealed (*FA*) specimens over the temperature and values found in MMPDS for annealed bar material

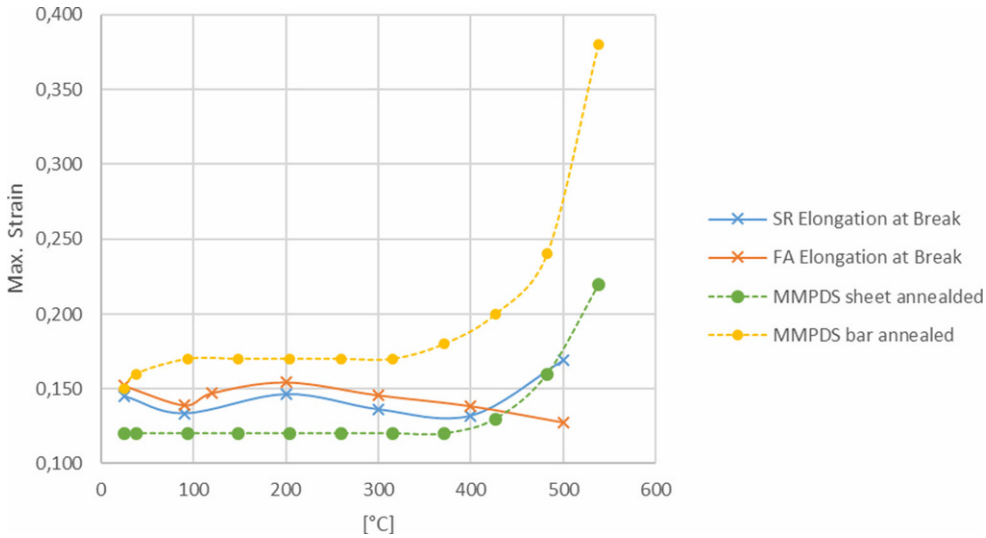

Fig. 5: Achieved maximal strain for stress-relieved (*SR*) and furnace-annealed (*FA*) specimens over the temperature and values found in MMPDS for annealed bar and sheet material

TABLE 4
Middle values and deviations for all tests performed

Temperature [°C]	Heat Treatment	Yield Strength [Mpa]	±	Ultimate Tensile Strength [Mpa]	±	Max. Strain	±
20	SR	1162	1	1205	1	0.145	0.002
	FA	1022	3	1083	5	0.152	0.009
90	SR	1023	3	1094	10	0.133	0.004
	FA	906	9	973	9	0.139	0.015
120	FA	874	2	941	10	0.147	0.000
200	SR	906	1	981	2	0.146	0.004
	FA	766	1	853	2	0.155	–
300	SR	845	13	903	18	0.136	0.001
	FA	698	2	793	2	0.146	–
400	SR	755	1	858	1	0.132	0.003
	FA	651	3	747	5	0.138	0.002
500	SR	695	7	756	12	0.169	0.001
	FA	591	7	656	17	0.128	0.007

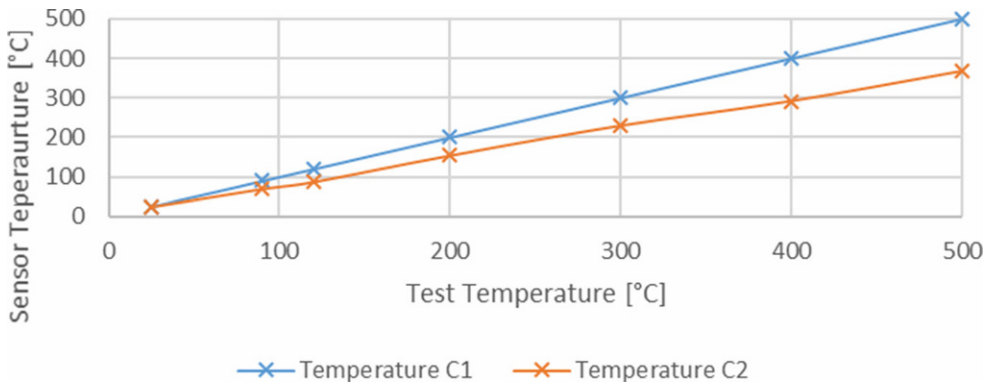

Fig. 6: Difference in temperature at thermocouple C1 (middle of gauge length) and C2 (end of gauge length)

show a strong increase in ductility from 400 °C on, as does max. strain for L-PBF stress-relieved samples.

The middle values and deviation of all results can be found in Table 4. Deviation for strength is very limited but is higher for the maximum strain reached.

Compared to the results from Zhao et al. [12], both heat treatments show a higher ductility and a smaller difference between yield and ultimate tensile strength. However, both decrease more with increasing temperature. Taking results from stress-relieved specimens, which are most similar to the ones in Zhao et al. [12], their UTS at room temperature is the same at 1200 MPa but just 858 MPa at 400° compared to 1016 MPa. Both show a loss in ductility for 400 °C, but with a nearly double elongation at break within our work (unclear: Zhao's or your contribution), 14 to 7.8% respectively. This might be because of the unclear orientation or missing stress-relief treatment in Zhao et al. [12]'sstudy.

Because Ti64 has a heat conductivity of just 7.1 W/mK, electric resistance heating leads to an increasing temperature gradient within the specimen. Figure 6 shows the difference between the temperature measured at the thermocouples placed at the beginning and end of the gauge length before the deformation.

4. Conclusions

The tensile strength reached by L-PBF Ti6A4V Grade 5 is higher than values in standards for forged and cast materials. Specimens with a partially martensitic microstructure show higher strength than furnace annealed specimens. The ductile behavior is found to be between furnace annealed bar and sheet material with $\alpha+\beta$ microstructure, well above SAE 4999 limits [20]. While more brittle at room temperature, stress-relieved samples approximate the ductility of furnace-annealed at higher temperatures, making martensitic α' Ti64 an interesting option at higher temperatures. In-depth studies of oxygen intake of martensitic α' depending on temperature are advisable as the limit for high-temperature application of Ti-Alloys lies in the oxygen intake and α-alloys are proven to withstand higher temperatures. Therefore resistance of martensitic α' Ti64 should be further investigated, since it can be produced by L-PBF without elaborate heat treatment.

As creep samples show anisotropy in ductility, a future investigation in this direction might be of interest for tensile and Charpy at elevated temperatures.

Due to the thermal properties, the samples at higher temperatures show large gradients in temperature over the specimen. Hence, the development of smaller size specimen standards would be of special interestas it already would be of great use for smaller L-PBF machines and if the availability of powder is limited.

Funding. Open access funding provided by Graz University of Technology.

References

1. Leyens, C., Peters, M.: Titanium and titanium alloys. Wiley-VCH, Hoboken (2003)
2. Lütjering, G., Williams, J.C.: Titanium, 2nd edn. Springer, Berlin, Heidelberg (2007)
3. Metallic Materials Properties Development and Standardization (MMPDS)-06, 2001, Chapter 5.4.1
4. Royer, F., Bienvenu, Y., Gaslain, F.: EBSD observation of grains microstructures produced by selective laser melting. In: Proceedings of the Conference Proceedings Euro PM2015, Reims, France, 4–7 September 2015 (2015)
5. Kunze, K., Etter, T., Grässlin, J., Shklover, V.: Texture, anisotropy in microstructure and mechanical properties of IN738LC alloy processed by selective laser melting (SLM). Mater. Sci. Eng. A **620**, 213–222 (2015)
6. Thijs, L., Sistiaga, M.L.M., Wauthle, R., Xie, Q., Kruth, J.-P., Van Humbeeck, J.: Strong morphological and crystallographic texture and resulting yield strength anisotropy in selective laser melted tantalum. Acta Mater **61**, 4657–4668 (2013)
7. Song, B., Dong, S., Coddet, P., Liao, H., Coddet, C.: Fabrication of NiCr alloy parts by selective laser melting: Columnar microstructure and anisotropic mechanical behavior. Mater Des **53**, 1–7 (2014)
8. Thijs, L., Verhaeghe, F., Craeghs, T., Van Humbeeck, J., Kruth, J.-P.: A study of the microstructural evolution during selective laser melting of Ti–6Al–4V. Acta Mater **58**, 3303–3312 (2010)
9. Yuxin, H., Yu'e, M., Weihong, Z., Zhenhai, W.: Effects of build direction on thermal exposure and creep performance of SLM Ti6Al4V titanium alloy. Eng. Fail. Anal. **135**, 106063 (2022). https://doi.org/10.1016/j.engfailanal.2022.106063
10. Viespoli, L.M., Bressan, S., Takamoto Itoh, T., Noritake Hiyoshi, N., Prashanth, K.G., Berto, F.: Creep and high temperature fatigue performance of as build selective laser melted Ti-based 6Al-4V titanium alloy. Eng. Fail. Anal. **111**, 104477 (2020). https://doi.org/10.1016/j.engfailanal.2020.104477
11. Muiruri, A.M., Maringa, M., Du Preez, W., Masu, L.: Variation of impact toughness of as-built Dmls TI6AL4V (ELI) specimens with temperature. S. Afr. J. Ind. Eng. **29**, 284–298 (2018)
12. Zhao, J.-R., Hung, F.-Y., Lui, T.-S., Wu, Y.-L.: The relationship of fracture mechanism between high temperature tensile mechanical properties and particle erosion resistance of selective laser melting ti-6Al-4V alloy. Metals **9**(5), 501 (2019). https://doi.org/10.3390/met9050501
13. Kuo, Y.-L., Horikawa, S., Kakehi, K.: Effects of build direction and heat treatment on creep properties of Ni-base superalloy built up by additive manufacturing. Scr Mater **129**, 74–78 (2017). https://doi.org/10.1016/j.scriptamat.2016.10.035
14. Lancaster, R.J., Davies, S.J., Jeffs, S.P., Lewis, D.T.S., Coleman, M.P.: The effects of thermal exposure on the high temperature behavior of a Laser Powder Bed Fused nickel based superalloy C263. Mater. Sci. Eng. A **801**, 140409 (2021). https://doi.org/10.1016/j.msea.2020.140409
15. Rao, V.R., Pattanayak, D.K., Vanitha, C.: Hot impression creep behavior of AlSi10mg alloy fabricated through SLM route. Trans Indian Inst Met (2022). https://doi.org/10.1007/s12666-022-02663-w
16. Meier, B., Godja, N., Warchomicka, F., Belei, C., Schäfer, S., Schindel, A., Palcynski, G., Kaindl, R., Waldhauser, W., Sommitsch, C.: Influences of surface, heat treatment, and print orientation on the anisotropy of the mechanical properties and the impact strength of Ti 6Al 4V processed by laser powder bed fusion. J. Manuf. Mater. Process. **6**, 87 (2022). https://doi.org/10.3390/jmmp6040087
17. Meier, B., Skalon, M., Warchomicka, F., Belei, C., Görtler, M., Kaindl, R., Sommitsch, C.: Effect of the reuse of powder on material properties of ti6Al4V processed by SLM. In: Proceedings of the AIP Confer-

ence Proceedings, Vitoria-Gasteiz, Spain, 8–10 May 2019, vol. 2113, p. 150006. (2019)
18. Powell, D., Rennie, A.E.W., Geekie, L., Burns, N.: Understanding powder degradation in metal additive manufacturing to allow the upcycling of recycled powder. J Clean Prod **268** (2020). https://doi.org/10.1016/j.jclepro.2020.122077
19. Bartolomeu, F., Gasik, M., Silva, F.S., Miranda, G.: Mechanical properties of ti6Al4V fabricated by laser powder bed fusion: a review focused on the processing and microstructural parameters influence on the final properties. Metals **12**, 986 (2022). https://doi.org/10.3390/met12060986
20. SAE-AMS4999; Issued 2002-02, Revised 2011-09, Reaffirmed 2016-09